Characterizing Fire-Induced Forest Structure and Aboveground Biomass Changes in Boreal Forests Using Multitemporal Lidar and Landsat

Tuo Feng, Laura Duncanson, Steven Hancock, Paul Montesano, Sergii Skakun, Michael A. Wulder, Joanne C. White, David Minor, and Tatiana Loboda

***Abstract*—Wildfire is the dominant stand-replacing disturbance regime in Canadian boreal forests. An accurate quantification of postfire changes in forest structure and aboveground biomass density (AGBD) provides a means to understand the magnitudes of ecosystem changes through wildfires and related linkages with global climate. While multispectral remote sensing has been extensively utilized for burn severity assessment, its capacity for postfire forest structure and AGBD change monitoring has been more limited to date. This study evaluates the interactions among burn severity, forest structure, and fire-return intervals for two representative sites in the western Canadian boreal forest. We adopted burn severity measurements from Landsat to characterize the heterogeneity of wildfire effects, while vertical forest structure information from Lidar was utilized to inform on realized forest changes and carbon fluxes associated with fire. Dominant trees in biomass-rich stands showed higher tolerance to low- and moderate-severity wildfires, while understory vegetation in these same stands showed a severity-invariant response to wildfires indicated by high vegetation mortality regardless of burn severity levels. Compared to a site without previous burn, canopy height and AGBD experienced lower magnitudes of change after subsequent wildfires, explained by a negative feedback between high frequency wildfires and biomass loss ($\overline{\Delta\text{Canopy Height}}_{\text{single wildfire}} = 3.03$ m; $\overline{\Delta\text{Canopy Height}}_{\text{successive wildfire}} = 2.47$ m; $\overline{\Delta\text{AGBD}}_{\text{single wildfire}} = 8.40$ Mg/ha; $\overline{\Delta\text{AGBD}}_{\text{successive wildfire}} = 6.69$ Mg/ha). This study provides new insights into forest recovery dynamics following fire disturbance, which is particularly relevant given increased fire frequency and intensity in boreal ecosystems resulting from climate change.**

***Index Terms*—Boreal forest, Landsat, Lidar, vegetation structure, wildfire.**

Manuscript received 21 August 2023; revised 17 November 2023 and 11 March 2024; accepted 29 April 2024. Date of publication 13 May 2024; date of current version 30 May 2024. This work was supported by NASA's Terrestrial Ecology Arctic Boreal Vulnerability Experiment Award 80NSSC19M0117 (PI Duncanson). *(Corresponding author: Tuo Feng.)*

Tuo Feng, Laura Duncanson, Sergii Skakun, David Minor, and Tatiana Loboda are with the Department of Geographical Sciences, University of Maryland, College Park, MD 20740 USA (e-mail: tuofeng@umd.edu; lduncans@umd.edu; skakun@umd.edu; minord@umd.edu; loboda@umd.edu).

Steven Hancock is with the School of Geoscience, University of Edinburgh, EH8 9XP Edinburgh, U.K. (e-mail: steven.hancock@ed.ac.uk).

Paul Montesano is with the Biosciences Laboratory, NASA Goddard Space Flight Center, Greenbelt, MD 20707 USA (e-mail: paul.m.montesano@nasa.gov).

Michael A. Wulder and Joanne C. White are with the Canadian Forest Service (Pacific Forestry Centre), Natural Resources Canada, Victoria, BC V8Z 1M5, Canada (e-mail: mike.wulder@Canada.ca; joanne.white@Canada.ca).

This article has supplementary downloadable material available at https://doi.org/10.1109/JSTARS.2024.3400218, provided by the authors.

Digital Object Identifier 10.1109/JSTARS.2024.3400218

I. Introduction

WILDFIRE is a common and natural disturbance agent in Canadian forests [1], impacting an average of 2.25 MHa of boreal forest annually [2]. These fires play an integrative role in influencing boreal species diversity, shaping the landscape patterns, and regulating biogeochemical cycling [3]. However, a rapidly increasing trend of fire-induced carbon emissions has been witnessed in the last few decades, and this trend is further predicted to escalate and exacerbate global climate change [4], [5]. Fire-induced carbon emissions can serve to increase CO_2 concentration in the atmosphere and thus enhance global warming trends which in turn have been shown to result in extended fire seasons, as well as increases in frequency and severity of wildfires [6]. A positive feedback loop is expected to further contribute to greenhouse gas emissions and global warming [7], [8], [9].

Burn severity, defined as the magnitude of ecological changes through wildfires [10], is a critical measurement to understand the effect of fires on vegetation succession processes and terrestrial carbon cycle [11]. Substantial variability of burn severity is expected to have different ecological consequences. Low-severity wildfire is defined as surface fires with less than 20% of overstory trees or basal area killed as the cumulative fire effects [12]. In boreal forests, low-severity burned areas are featured with scorched or lightly charred surfaces with minimal organic matter consumption and overstory mortality [13]. Combustion of understory vegetation through low-severity fires enables penetration of sunlight to the forest floor and supports the growth of seedlings and saplings. Conversely, the occurrence of high-severity fire can shift the successional trajectories of dominant species [14], and catalyze conversions from forested to nonforested landscapes [15].

Multispectral remote sensing has been widely recognized as an efficient technique to evaluate wildfire effects in a spatially-explicit and consistent manner [16], [17]. The normalized burn ratio (NBR) is a spectral index first introduced by Key and Benson [10] for remotely sensed burn severity mapping. This index was developed based on the concept that the near-infrared (NIR; 0.76–0.90 μm) and shortwave infrared (SWIR; 2.08–2.35

μm) channels from Landsat 5 Thematic Mapper (TM) demonstrated sensitive but inverse responses to mesophyll structure and surface moisture content. NBR can capture the heterogeneity of postfire effects and several studies have integrated NBR from air- and space-borne optical sensors for the assessment of burn severity levels at regional [18], national [19], and global scales [20], [21]. Delta NBR (dNBR; [10]) and relative dNBR (RdNBR; [22]) were further constructed by combining NBR measurements pre- and postfire to reflect the magnitudes of changes through wildfire relative to prefire conditions. In parallel with multispectral burn severity indices, composite burn index (CBI) was also developed by Key and Benson [10] as a standard field-based protocol for burn severity assessments. CBI is measured through a visual assessment of change of multiple factors (e.g., soil charring, vegetation consumption, etc.) across five height strata and within a 30 m $\times$ 30 m sample plot, thereby providing a comprehensive evaluation of fire effects on forest change [23], [24]. Varying levels of success have been achieved in establishing linkages between CBI and remotely sensed burn severity indices in boreal forests [25], [26], [27], [28], [29]. For example, Allen and Sorbel [25] assessed the correlation between dNBR and CBI for 10 wildfires that occurred in the Alaska boreal regions. R^2 values were found to range between 0.45 and 0.88 with the strength of correlation dependent upon species types, burn severity levels, and date of field assessment. The dNBR-CBI correspondence was also evaluated in western Canadian boreal forests and the robustness of linkages was found to vary with respect to driving variables including fuel type and statistical models established [27]. Although burn severity measurements from multispectral imagery have demonstrated potential for capturing the variability of postfire effects [13], [30], the uncertainties associated with CBI remain, primarily due to difficulty deconvolving the potential variety of fire impacts on a single grid cell measurement. Interpretation of burn severity indices from multispectral imagery is also tenuous due to the lack of biometric definitions associated with them [31]. Due to this challenge, a connection between remote sensing-based burn severity measurements and forest structural changes enables our quantitative evaluation of forest losses and aboveground biomass fluxes through fires.

An accurate characterization of fire-induced forest aboveground biomass density (AGBD) change is important to unveil the relationships between wildfire and forest carbon dynamics [32]. However, the remoteness and low accessibility of large swaths of Canadian boreal forests prohibit the development of field inventory with broad spatial and temporal extents, thereby limiting our direct assessments of the fire-induced structural and AGBD dynamics. Previous studies have found strong associations between AGBD and forest structure parameters (e.g., canopy height, cover, etc.) directly retrieved from Lidar (light detection and ranging) observations [33], [34]. Therefore, monitoring the three-dimensional (3-D) structure change with Lidar could by a means to deliver reliable assessments of fire-induced aboveground carbon loss.

Lidar is a popular technology for forest structure and biomass mapping [35], [36], [37], [38]. In the context of wildfire effects assessment, multitemporal Lidar measurements have been primarily adopted to capture the variation of vegetation structure through the change of various Lidar-derived structural metrics. For example, Karna et al. [39] employed bi-temporal airborne discrete-return Lidar (DRL) to monitor the forest structural change through fire and they found significant decreases in canopy height and cover. Although some efforts have been made to explore forest structure response to wildfires with Lidar, most studies either focused on a single wildfire without considering previous fire disturbance history [9], [40], [41], [42] or excluded regions with high-intervals fires to avoid the compound effect from previous burns [43]. However, the interactions between successive wildfires, and their compound effects on forest change can provide additional insights into ecosystem resilience and terrestrial carbon budgets. Some pioneering studies have been conducted to analyze interactions between successive wildfires and their joint effects on the ecological changes, as measured by burn severity [24], [44], [45]. However, results found in those studies were mixed suggesting the effects of previous and high-frequency fires on burn severity levels of subsequent wildfire can be either positive or negative contingent upon multiple drivers (e.g., forest zone, regeneration rate, intervals between successive fires, etc.) and their quantitative relationships are largely unknown. Therefore, additional investigation is required to understand the relationships between fire frequency, severity, and biomass change. Here, we aim to provide a spatially explicit characterization of forest vertical structure and AGBD changes and analyze the drivers of the forest changes. The objectives of this article are as follows.

1) To explore the relationship between burn severity, fire-induced forest structure, and AGBD change at two study sites in Canada's boreal ecosystem.
2) To understand how prefire forest structure and AGB contents impact the magnitudes of height change and carbon fluxes through fire.
3) To evaluate the impacts of fire-return interval on the magnitude of forest losses through wildfires.

II. Study Area

The Canadian boreal ecosystem constitutes an area of $\sim$552 million ha, with $\sim$270 million ha of treed lands [46]. These forest ecosystems encompass broad ecological and environmental gradients and play a fundamental role in climate mitigation and biodiversity conservation [47], [48] The first study site of this work straddles the border of Northwest Territories and Saskatchewan, at southwestern edge of Taiga Shield ecozone [49]. This region is categorized as a subarctic climate [50] with January and July mean temperature of -20.4 °C and 16.9 °C, respectively [51]. Evergreen needleleaf forests are widely distributed across the site with dominant species including black spruce (*Picea mariana*) and jack pine (*Pinus banksiana*) [52]. No previous fire has been recorded at this location from available records within the Canadian Large Fire Database except the one that occurred between June 2nd and July 12th of 2011 with burned areas of approximately 64184 ha [53]. The second site is in northern Saskatchewan and within the Boreal Shield ecozone [49]. Tree species within our second site are more homogeneous

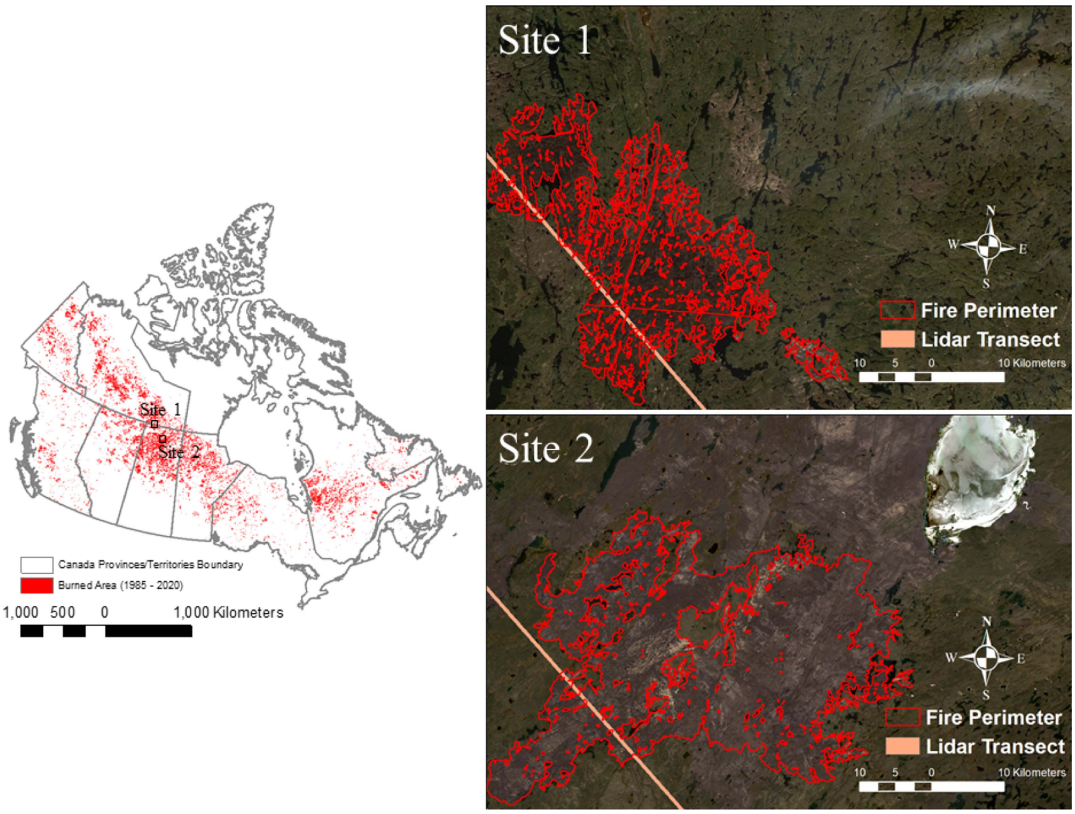

Fig. 1. Geographical domain of study sites and fire perimeters. Postfire Landsat imagery was acquired on May 20th, 2013 (Site 1; Landsat 5 TM shown as Band 4, 3, 2 composite) and May 21st, 2015 (Site 2; Landsat 8 OLI shown as band 5, 4, 3 composite).

with black spruce (*Picea mariana*) dominating. Subdominant species include jack pine (*Pinus banksiana*) and trembling aspen (*Populus tremuloides*). We consider this site as an example of a short-interval fire, given two wildfires occurred within the past 25 years (1995 and 2013) with 87 398 ha and 113 895 ha burned, respectively. The geographic domains of both study sites are shown in Fig. 1.

III. Data and Method

A. Airborne Lidar Data

The multitemporal airborne Lidar acquired pre- and postfire were incorporated to observe the magnitude of fire-induced forest structure and biomass changes. The first airborne Lidar campaign was carried out during the summer of 2010 resulting in 34 transects with a total length of 24 286 km [54]. The small-footprint discrete return data were collected by an Optech ALTM 3100 laser scanner equipped on a fixed-wing aircraft with the flying altitude of ∼1200 m above ground level [55]. Operated at a 70 kHz pulse rate and 1064 nm wavelength, the sensor has a scan angle of ±15° from nadir and a nominal pulse density of ∼2.8 returns/m^2 was yielded with an expected nominal footprint size of ∼30 cm [54].

The postfire Lidar data were acquired by land, vegetation, and ice sensor (LVISs) during June–August 2019 across northern Canada and Alaska as part of the NASA's Arctic-Boreal Vulnerability Experiment airborne campaign [56]. The LVIS instruments (i.e., LVIS-Classic; LVIS-Facility) are large-footprint full-waveform laser ranging systems operated with a wavelength centered at 1064 nm and with a pulse width of 5 nm. The nominal footprint diameters of LVISs are ∼10 m (LVIS-Facility) and ∼25 m (LVIS-Classic), respectively. The laser altimeters were aboard the NASA Gulfstream V plane with a flight altitude of ∼8 km and scanning angle of ±8° around nadir [57] yielding a nominal swath width of ∼2.5 km. LVIS-facility with its smaller footprint is more directly comparable to the discrete return 2010 Lidar. In this work, we adopted LVIS-Facility Level 1B [58] and Level 2 [59] datasets containing footprint-level geolocated return energy waveforms and height metrics describing terrain elevation and vertical structure of forest canopy, respectively.

B. Landsat

Landsat imagery representing conditions present pre- and postfire were adopted to generate burn severity measurements. We adopted the image selection strategies proposed in [60] to extract high-quality Landsat scenes in term of

1) minimum amount of cloud and cloud shadows contamination within the burned scars,
2) combinations of Landsat sensors for pre- and postfire imagery acquisition (i.e., TM-TM, OLI-OLI), and
3) preference of close acquisition date during the growing season given similar phenology conditions.

Since the wildfire in our first site occurred months before the failure of Landsat 5 TM (November 2011), whereas the second one soon after the operation of Landsat 8 OLI (February 2013), the availability of image pairs are limited. Despite that, cloud-free imagery with the closest date of acquisition was chosen at both sites. We selected image pairs (Path 42, Row 18) from Landsat 5 TM pre- (June 23rd, 2008) and postfire (July 18th, 2011) across the first study site, and bi-temporal Landsat 8 OLI data (Path 39, Row 20) pre- (May 31st, 2013) and postfire (May 21st, 2015) to characterize the change of surface conditions through fire at the second study site. All Landsat imagery was processed to Collection 2 surface reflectance product through USGS ESPA.[1]

C. Ancillary Data

This study used national burned area composite (NBAC) to independently capture fire perimeters across our two study sites. NBAC consists of the spatially-explicit representation of the extent, duration, and frequency of burned areas in Canada on an annual basis since 1986 [53]. Since two wildfires occurred at the second site in 1995 and 2013, we further classified the fire perimeters based on fire-return intervals with areas burned once and twice categorized as low- and high-fire frequency regions, respectively.

D. Waveform Simulation and Structural Metrics Extraction

In order to facilitate the direct measurement of fire-induced forest structural change, a waveform simulation procedure was first carried out to convert the 2010 DRL within each LVIS-Facility footprint to a simulated waveform through the GEDI simulator [57], which is dependent upon the original algorithm developed in [61]. Since small- and large-footprint Lidar adopted in this study has unique sensor characteristics (e.g., footprint diameter, pulse length; intensity, etc.), a conversion from DRL to the pseudo-LVIS waveform is a prerequisite for making the multitemporal Lidar datasets directly comparable. The DRL point cloud acquired from the 2010 airborne campaign was extracted per LVIS-Facility footprint and simulated to the waveform through footprint-level convolution [62] given the energy contribution of individual discrete return points along and across the laser beam following the Gaussian distribution. Since the footprint diameter of LVIS-Facility is highly variable and dependent upon the flying altitude during data acquisition, discrete-return datasets were moved along an error surface based on a preset horizontal and vertical offsets to find the best affine transformation and footprint size [57]. Note that the full collection of along-track footprints is shifted together, and individual footprints are not shifted independently. The postfire footprint-level structural metrics stored in LVIS Level 2 files were employed and paired with prefire metrics extracted from simulated waveforms for our change analysis. First, we calculated the average bias and root mean squared error (RMSE) of terrain height from multitemporal Lidar to ensure both datasets were properly collocated. The differences in Lidar attributes were then obtained to characterize the magnitude of forest structure change through a wildfire. That includes multiple relative height (RH) metrics (i.e., RH98; RH90; RH80; RH60; RH50) representing the proportion of waveform energy occurring relative to ground. The RH98 was used in this work to represent canopy height due to its reduced sensitivity to noise [57]. In addition, we estimated footprint-level AGBD through the generalized boreal-wide LVIS biomass model calibrated by field inventory data throughout North America boreal [63], which generally followed the methods developed for NASA's Global Ecosystem Dynamics Investigation mission [36], but with field and airborne Lidar collected for boreal forests. These models are generalized based on continent and broad vegetation classes (deciduous and needleleaf forests), and a boreal-wide model was applied for this study that predicts aboveground biomass as a function of waveform metrics, in this case RH98 (maximum height) and RH70.

E. Burn Severity Measurements

The spectral indices from multitemporal Landsat imagery were utilized to characterize burn severity for the two study sites. We calculated the three most widely used burn severity indices: NBR, dNBR, and RdNBR through the following equations:

$$\mathrm{NBR} = (\mathrm{Band}_{\mathrm{NIR}} - \mathrm{Band}_{\mathrm{SWIR2.1}}) / (\mathrm{Band}_{\mathrm{NIR}} + \mathrm{Band}_{\mathrm{SWIR2.1}}) \tag{1}$$

$$\mathrm{dNBR} = \mathrm{NBR}_{\mathrm{prefire}} - \mathrm{NBR}_{\mathrm{postfire}} \tag{2}$$

$$\mathrm{RdNBR} = \mathrm{dNBR} / \sqrt{\mathrm{ABS}\,(\mathrm{NBR}_{\mathrm{prefire}})} \tag{3}$$

where $\mathrm{Band}_{\mathrm{NIR}}$ and $\mathrm{Band}_{\mathrm{SWIR2.1}}$ denote surface reflectance of NIR and shortwave-infrared (SWIR 2) channels from Landsat data. Taking the absolute value of prefire NBR allows our calculation of the square-root in the denominator without changing the sign if the original dNBR dropped to negative [22]. All the spectral indices were scaled up by a factor of 10 000 to improve the interpretability of burn severity gradients.

F. Geospatial Analysis

Patch-level analysis was adopted in this study to evaluate the relationship between forest changes and burn severity levels. To achieve this, we segmented the Normalized Difference Vegetation Index (NDVI, [64]) from postfire Landsat imagery using mean shift image algorithm [65], [66]. The mean shift is an image segmentation technique that clusters pixels within a searching radius based on mathematical morphological theories for region growths. The algorithm uses a kernel function to specify the weight of nearby points to iteratively estimate the mean of the clusters. We used the ArGIS implementation of the mean shift algorithm, which included a Gaussian kernel function. We set up both the spatial and spectral detail parameters to 10 (range from 1.0 to 20.0) for equalized contributions from spatial and spectral information to the segmentation results [67], [68]. Each segment represents an individual analysis unit occupied by a homogeneous forest layer while all the pixels

[1][Online]. Available at: https://espa.cr.usgs.gov/

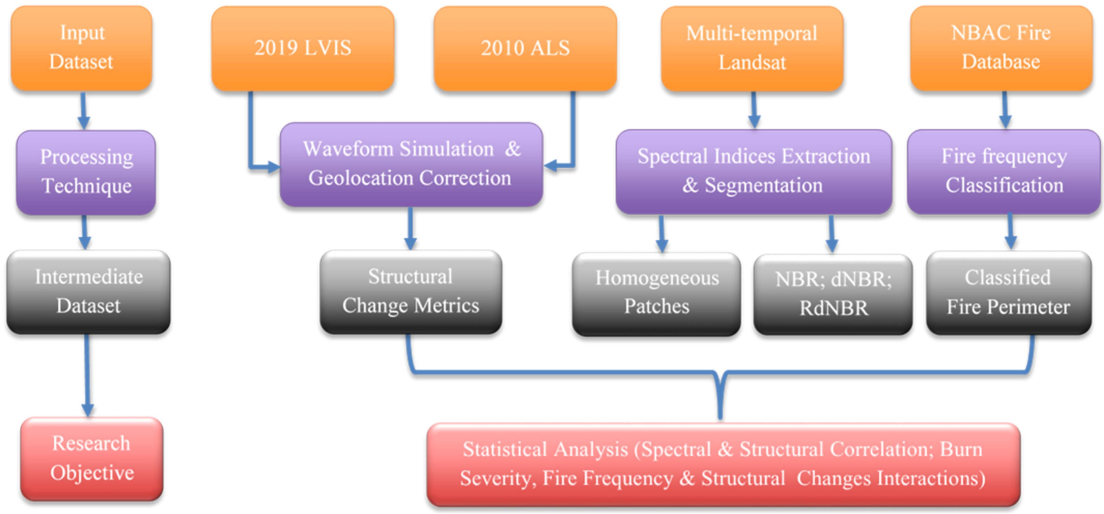

Fig. 2. Methodological workflow for this study.

within a single patch are characterized by strong spectral and spatial similarities. The mean of postfire Lidar attributes (e.g., AGBD, Canopy Height, dNBR, etc.), and the magnitude of attribute changes (i.e., Absolute change: Prefire metrics–Postfire metrics; Relative changes: (Prefire metrics–Postfire metrics) / Prefire metrics) were calculated within each homogeneous patch and correlated with segment-level burn severity indices from pre- and postfire Landsat imagery. We adopted the linear regression model to assess spectral–structural relationships with the strength of correlation measured by Pearson correlation coefficient. It should be noted, however, that the majority of segments spatially overlap both short- and long-interval fire perimeters, which constrained our use of patch-level analysis to assess the effects of fire frequency on forest damages. To address this issue, per-pixel analysis was adopted in the last step to further quantify the interactions among fire-return intervals, burn severity, and magnitude of forest change through fire. Specifically, the pre-, postfire, and absolute change of Lidar attributes were gridded to 30 m spatial resolution and spatially matched with classified burn severity maps. The burn severity maps were categorized as low-, moderate- and high-severity based on the dNBR thresholds developed in [27] suitable for postfire effect characterizations across Canadian boreal forests (i.e., Low severity: $410 < \text{dNBR} < 2830$; Moderate severity: $2830 < \text{dNBR} < 5130$; High severity: $\text{dNBR} > 5130$). The Lidar attributes and classified burn severity maps were further masked by fire frequency perimeters, yielding two sections with wildfires burned once and twice respectively. We adopted an independent two-sample *t*-test to evaluate the strength and significance of forest structure and AGBD change with respect to fire-return intervals and burn severity levels. The methodological workflow of this study is shown in Fig. 2.

IV. Result

Overall, multitemporal Lidar transects comprised 292 and 653 ha of burned area within the first and second study sites. Site 1 is characterized by higher prefire forest canopy and AGBD, along with more vegetation occupying the understory (see Table I). This can be attributed to the effects of low-frequency wildfires in site 1, which provides sufficient time for forest regrowth postdisturbance. Fig. 3 summarizes the comparison of footprint-level terrain elevation and canopy height from multitemporal Lidar. High coincidence of terrain elevation was found across two sites pre- and postfire ($\text{RMSE}_{\text{site 1}} = 0.54$ m; $\text{bias}_{\text{site 1}} = 0.25$ m; $\text{RMSE}_{\text{site 2}} = 0.28$; $\text{bias}_{\text{site 2}} = 0.13$ m), indicating both datasets were properly collocated for subsequent change analysis. For an illustration of canopy height change [see Fig. 3(b) and (d)], we filtered out footprints with RH98 lower than 1.37 from the original scatterplots [see Fig. S1(a) and (b)]. This process is to remove all non-forest footprints through this threshold broadly used to discern trees from shrubs in boreal forest [69], and further highlight the post-fire effects as described by the dramatic decrease of canopy height. Overall, 86% (site 1) and 83% (site 2) of footprints experienced a height decrease associated with wildfires, with mean height loss of 3.14 m and 2.61 m, respectively. This decrease in canopy height is primarily attributed to the dominance of some evergreen conifer species (e.g., Black Sprice; Jack Pine, etc.) across our two study sites, which are highly flammable and less resistant to wildfires. These conifer-dominated stands would experience high mortality rates through fires, and even being fully removed, demonstrated as the stand-replacing effect.

The distribution of burn severity indices inside and outside NBAC fire perimeters, as shown in Fig. 4, described the wildfire effects on land surface change captured by multitemporal Landsat. We observed significant differences in all burn severity indices with the presence and absence of fire across both study sites, given burned areas displaying much higher dNBR against regions of absence of fire (see Table I). In site 2, the burn severity indices across different fire frequency classes were compared through an independent two-sample *t*-test. Marked differences ($p<0.0001$) were found for all burn severity indices within short- and long-interval fire regions, which indicates the presence of previous and short-interval wildfires on burn severity variabilities of subsequent burns.

TABLE I
SUMMARY OF FOREST AND FIRE CHARACTERISTICS ASSOCIATED WITH TWO STUDY SITES

Site-level Characteristic	Site 1	Site 2
Burned area with lidar coverage # of lidar footprints	292 ha 80 927	653 ha 33 243
# of homogeneous patches Mean Patch Size Standard Error of Patch Size	249 Mean = 3.94 ha SE = 0.52 ha	122 Mean = 3.98 ha SE = 0.65 ha
Mean/Standard Error of pre-fire Canopy Height (RH98)	Mean = 4.86 m SE = 0.02 M	Mean = 4.43 m SE = 0.05 m
Mean/Standard Error of pre-fire RH50	Mean = 0.76 m SE = 0.007 m	Mean = 0.15 m. SE = 0.005 m
Mean/Standard Error of pre-fire AGBD	Mean = 11.11 Mg/ha SE = 0.09 Mg/ha	Mean = 9.74 Mg/ha SE = 0.16 Mg/ha
Mean post-fire NBR/dNBR/RdNBR within fire perimeter	NBR = -117 dNBR = 1782 RdNBR = 4349	NBR = -1947 dNBR = 3890 RdNBR = 3120
Mean post-fire NBR/dNBR/RdNBR outside fire perimeter	NBR = 926 dNBR = 171 RdNBR = -68	NBR = 1565 dNBR = 768 RdNBR = 676
Mean and Standard Error of terrain slope	Mean = 4.09° SE = 0.04 °	Mean = 1.87°. SE = 0.03°

A. *Correlations Between Structural and Spectral Attributes*

Through implementations of the mean shift segmentation algorithm (ArcMap 10.6) on postfire NDVI, we derived 249 (site 1) and 122 (site 2) segments, respectively. Each segment represents a homogeneous forest layer characterized by strong spectral and spatial similarities. The correlations between structural and spectral metrics, as illustrated in Tables II and III, varied in direction, magnitude, and significance. In site 1, dNBR demonstrated a strong correlation with both absolute and relative changes of Lidar attributes, primarily those describing structural characteristics of upper canopy layers (i.e., RH98; RH90, RH80). Postfire NBR and RdNBR showed reasonable linkages with absolute and relative changes of AGBD as well as those high RH metrics ($0.338 < |r| < 0.641$). Conversely, we observed weak relationships between burn severity indices and lower RH metrics ($0.016 < |r| < 0.538$). This contrasting result can be attributed to the limited capacity of multispectral imagery on understory change detection, particularly in multilayered forest with complex vertical structures. The dNBR demonstrated robust linkages with relative changes of AGBD and high RH metrics (i.e., RH98; RH90, RH80) in our second site ($0.731 < |r| < 0.838$). We also noticed strong correlations (pearson's $r > 0.5$ and $p < 0.001$) among all spectral indices and low RH metrics (i.e., RH70; RH60, RH50) acquired from postfire Lidar. This contrasting performance of burn severity indices on understory change detection could be attributed to the differences in vertical complexity between the two study sites, particularly given site two experienced short-interval wildfires, along with limited time for recovery postdisturbance.

B. *Impacts of Prefire Structure on Forest Losses*

Fig. 5 illustrates the postfire AGBD and canopy structure with respect to the prefire condition and burn severity gradients, as described by dNBR. At both study sites, we observed a consistent pattern regarding the forest structure and biomass responses to wildfire. Segment-level mortality varies across tree height gradients with taller and more mature stands showing low levels of mortality in low-severity fire and high level of mortality in high-severity sections of the burn. In contrast, mortality of short vegetation (immature trees and other understory species) appears to be burn-severity insensitive given the higher strength of AGBD and structure changes relative to prefire conditions. In short, lower RH metrics (low vegetation) are more sensitive to low-severity fires, while high RH metrics are relatively insensitive to low-severity fires but sensitive to high-severity fires. It should be noted that, due to differences in Lidar platforms

TABLE II
SEGMENT-LEVEL LINEAR CORRELATION (PEARSON CORRELATION COEFFICIENT (R) AND P-VALUE) BETWEEN LANDSAT-DERIVED SPECTRAL INDICES AND LIDAR ATTRIBUTES IN SITE 1

Site 1: Northwest Territory Variable	Postfire (2011)			Absolute Change (Prefire – Postfire)			Relative Change (Prefire — Postfire)/Prefire		
	NBR	dNBR	RdNBR	NBR	dNBR	RdNBR	NBR	dNBR	RdNBR
AGBD (Mg/ha)	0.162	–0.129	–0.11	–0.477	0.478	0.338	**–0.628**	**0.647**	**0.546**
	0.010	0.041	0.089	$p < 0.001$	$p < 0.001$	$p < 0.001$	**$p < 0.001$**	**$p < 0.001$**	**$p < 0.001$**
Canopy Height (m)	0.180	–0.135	–0.127	**–0.614**	**0.604**	0.443	**–0.641**	**0.629**	**0.531**
	0.004	0.034	0.046	**$p < 0.001$**	**$p < 0.001$**	$p < 0.001$	**$p < 0.001$**	**$p < 0.001$**	**$p < 0.001$**
RH90 (m)	0.180	–0.161	–0161	**–0.604**	**0.629**	0.494	**–0.609**	**0.655**	**0.581**
	0.004	0.011	0.011	**$p < 0.001$**	**$p < 0.001$**	$p < 0.001$	**$p < 0.001$**	**$p < 0.001$**	**$p < 0.001$**
RH80 (m)	0.182	–0.187	–0.193	**–0.538**	**0.601**	**0.501**	**–0.551**	**0.645**	**0.607**
	0.004	0.003	0.002	**$p < 0.001$**	**$p < 0.001$**	**$p < 0.001$**	**$p < 0.001$**	**$p < 0.001$**	**$p < 0.001$**
RH70 (m)	0.171	–0.195	–0208	–0.456	**0.545**	0.466	–0.423	**0.547**	**0.573**
	0.007	0.002	0.001	$p < 0.001$	**$p < 0.001$**	$p < 0.001$	$p < 0.001$	**$p < 0.001$**	**$p < 0.001$**
RH60 (m)	0.170	–0.204	–0.231	–0.392	0.496	0.423	–0.040	–0.060	–0.042
	0.007	0.001	$p < 0.001$	$p < 0.001$	$p < 0.001$	$p < 0.001$	0.535	0.350	0.507
RH50 (m)	0.172	–0.220	–0.254	–0.419	**0.538**	0.463	–0.016	0.030	0.095
	0.007	$p < 0.001$	$p < 0.001$	$p < 0.001$	**$p < 0.001$**	$p < 0.001$	0.823	0.640	0.134

In bold: pearson correlation coefficient (r) > 0.5 and α = 0.05

TABLE III
SEGMENT-LEVEL LINEAR CORRELATION BETWEEN LANDSAT-DERIVED SPECTRAL INDICES AND LIDAR ATTRIBUTES IN SITE 2

Site 2: Saskatchewan Variable	Postfire (2011)			Absolute Change (Prefire — Postfire)			Relative Change (Prefire — Postfire)/Prefire		
	NBR	dNBR	RdNBR	NBR	dNBR	RdNBR	NBR	dNBR	RdNBR
AGBD (Mg/ha)	0.316	–0.488	–0.404	–0.428	0.304	0.455	**–0.704**	**0.812**	**0.790**
	0.001	$p < 0.0001$	$p < 0.0001$	$p < 0.0001$	0.001	$p < 0.0001$	**$p < 0.0001$**	**$p < 0.0001$**	**$p < 0.0001$**
RH98/Canopy Height (m)	0.337	**–0.526**	–0.415	–0.568	**0.527**	**0.631**	**–0.703**	**0.838**	**0.790**
	0.0002	**$p < 0.0001$**	$p < 0.0001$	$p < 0.0001$	**$p < 0.0001$**	**$p < 0.0001$**	**$p < 0.0001$**	**$p < 0.0001$**	**$p < 0.0001$**
RH90 (m)	0.371	**–0.545**	–0.475	–0.430	0.323	0.466	**–0.702**	**0.783**	**0.802**
	$p < 0.0001$	**$p < 0.0001$**	$p < 0.0001$	$p < 0.0001$	0.0005	$p < 0.0001$	**$p < 0.0001$**	**$p < 0.0001$**	**$p < 0.0001$**
RH80 (m)	0.392	**–0.529**	–0.483	–0.313	0.162	0.295	**–0.719**	**0.731**	**0.769**
	$p < 0.0001$	**$p < 0.0001$**	$p < 0.0001$	0.001	0.087	0.002	**$p < 0.0001$**	**$p < 0.0001$**	**$p < 0.0001$**
RH70 (m)	**0.558**	**–0.594**	**–0.577**	–0.210	0.034	0.153	**–0.718**	**0.685**	**0.701**
	$p < 0.0001$	**$p < 0.0001$**	**$p < 0.0001$**	0.027	0.718	0.108	**$p < 0.0001$**	**$p < 0.0001$**	**$p < 0.0001$**
RH60 (m)	**0.585**	**–0.557**	**–0.555**	–0.249	0.131	0.216	–0.462	0.489	0.434
	$p < 0.0001$	**$p < 0.0001$**	**$p < 0.0001$**	0.008	0.168	0.022	$p < 0.0001$	$p < 0.0001$	$p < 0.0001$
RH50 (m)	**0.583**	**–0.549**	**–0.550**	–0.341	0.235	0.309	–0.033	0.007	0.021
	$p < 0.0001$	**$p < 0.0001$**	**$p < 0.0001$**	=0.0002	0.013	0.001	0.733	0.945	0.822

In bold: pearson correlation coefficient (r) > 0.5 and α = 0.05.

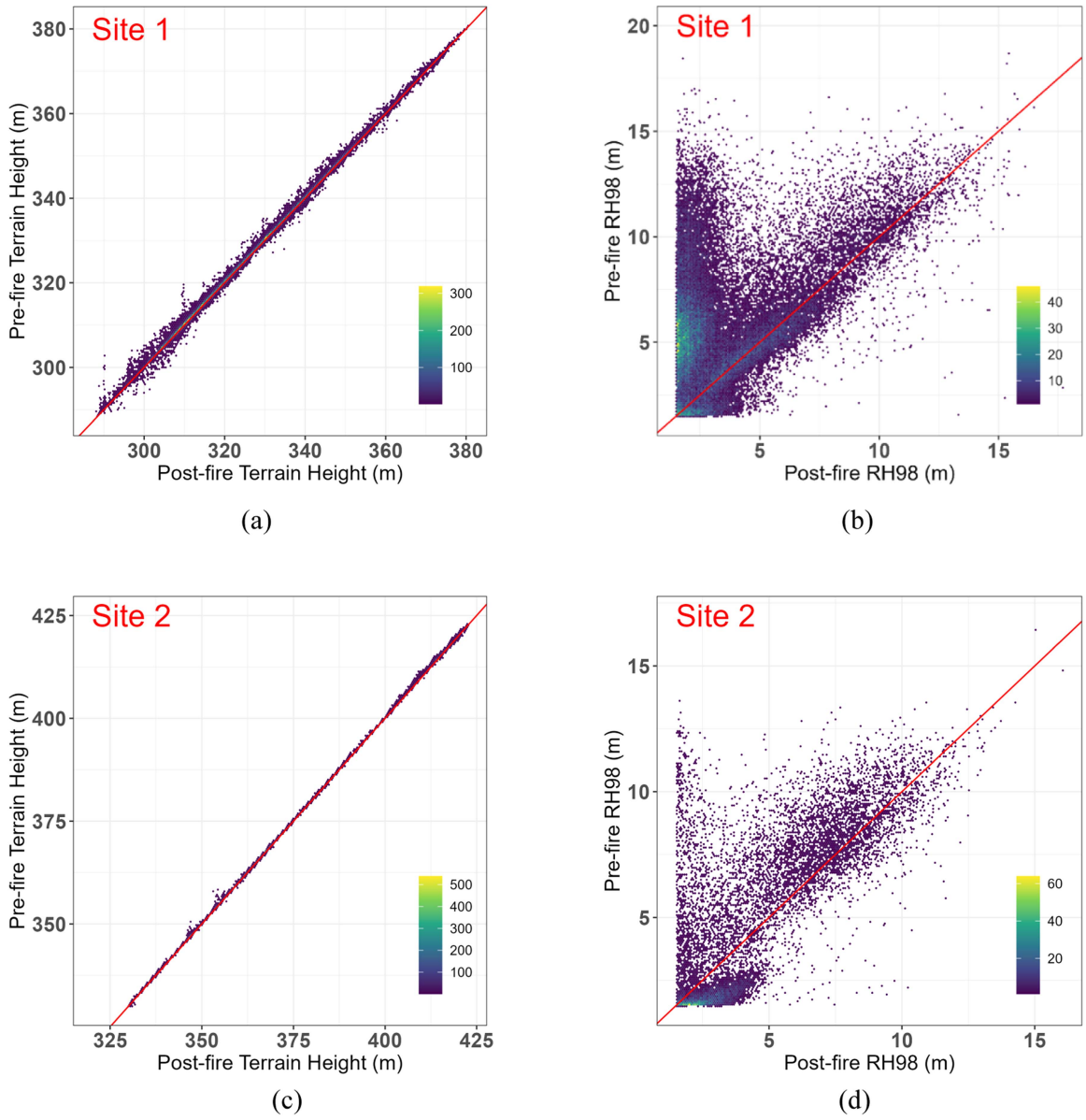

Fig. 3. Footprint-level comparison of terrain elevation (a; c) and canopy height (b; d) between 2010 ALS and 2019 LVIS-Facility across site 1 (a; b) and site 2 (c; d). Site 1 (a; b) was burned in 2011 (June 2nd–July 12th) and site 2 (c; d) was burned in 1995 (May 29th–July 6th) and 2013 (July 4th - Sep 8th).

adopted for pre- and postfire data acquisitions, slight discrepancies existed when comparing changes in Lidar attributes through fire. Particularly, the RH of understory vegetation (RH50; RH60) within some segments was found to be negative at pre- or postfire stage. This can be attributed to the loss of canopy cover through the fire, thereby altering the shapes of waveform with RH50 dropped below the mean elevation of the lowest detected mode (ZG).

C. Effects of Fire-Return Interval on Magnitude of Forest Damages

The pre-, postfire, and absolute change of Lidar attributes across short- and long-interval fire regions in site 2 were compared, as illustrated in Table IV. Overall, 6780 and 12 030 LVIS footprints fall within the perimeters of short- and long -interval wildfires, occupying burned areas of 103 ha and 188 ha respectively. At the prefire stage, Lidar attributes describing structural characteristics of overstory (RH90) and understory (RH60; RH50) were found to be significantly different relative to fire-frequency, as reflected by short-interval burned areas with lower RH values. These can be attributed to the effects of previous and high-frequency wildfires, which limited the time of forest recovery and fuel accumulation before subsequent burns. Interestingly, we found all metrics postfire and change through fire were significantly different ($p < 0.05$) with respect to the presence and absence of previous burns. Among all attributes considered, fire-return intervals demonstrated the most prominent impacts on postfire and absolute change of AGBD and high RH metrics (RH98; RH90) ($4.80 < t < 7.33$), while the strength

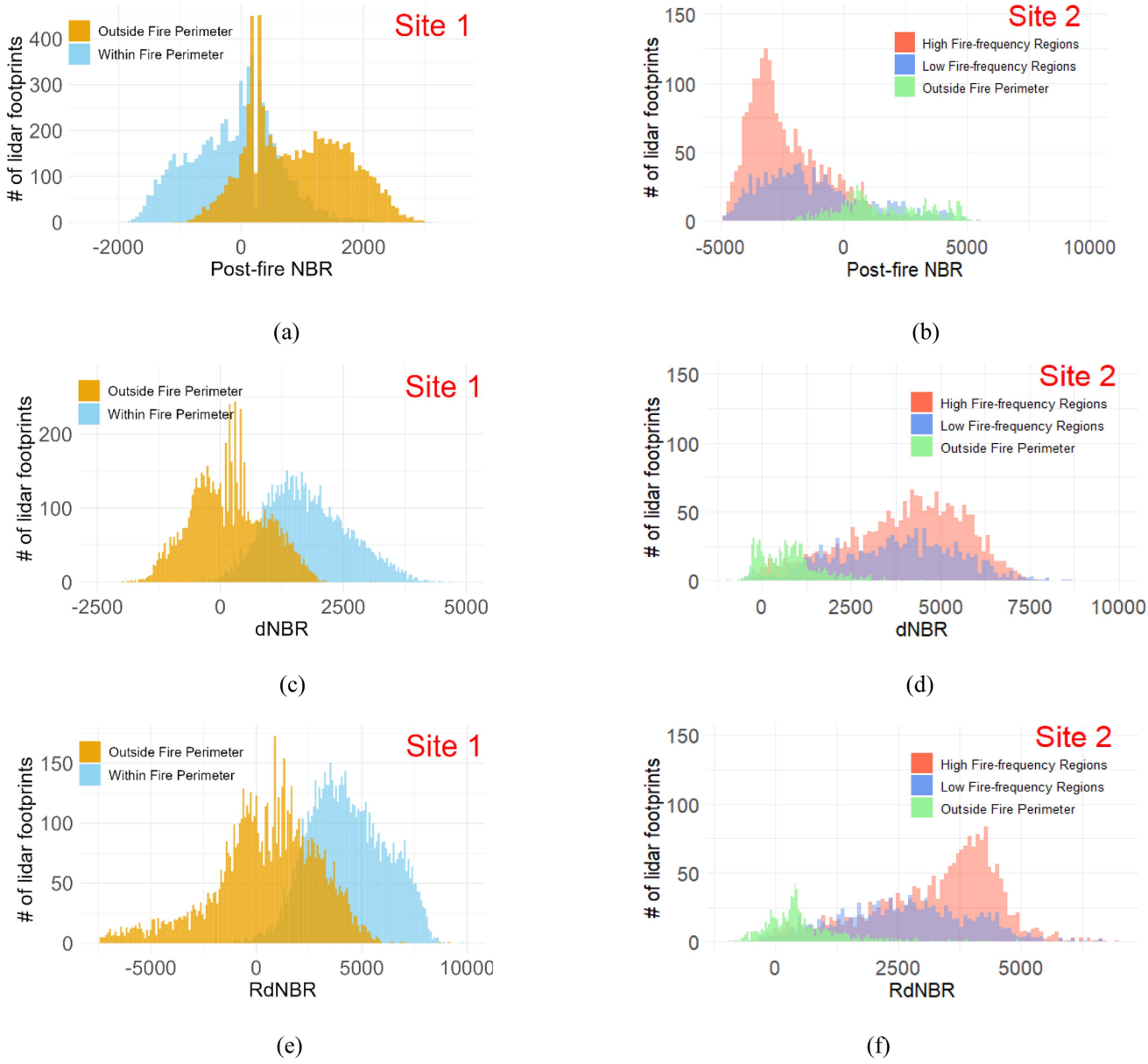

Fig. 4. Distribution of scaled Landsat-derived post-fire NBR (a; b), dNBR (c; d) and RdNBR (e; f) in site 1 (a; c; e) and site 2 (b; d; f).

of this difference reduced for those low RH metrics (RH70; RH60; RH50), as described by the *t*-value ranging from 2.28 to 4.78.

The magnitudes of AGBD and canopy height change across prefire attribute gradients are illustrated in Fig. 6. Overall, changes in AGBD and canopy height demonstrated consistent trends with respect to fire-return intervals and burn severity levels. Within the perimeter of low severity fire ($430 < \text{dNBR} < 2830$), the reburned areas experienced a lower degree of AGBD and canopy height changes across prefire gradients, particularly in high-biomass stands occupied by large trees (Mean $\Delta \text{AGBD}_{\text{High Fire Frequency and Prefire AGBD} > 35\ \text{Mg/ha}} = 15.98$ Mg/ha; Mean $\Delta\text{AGBD}_{\text{Low Fire Frequency and Prefire AGBD} > 35\text{Mg/ha}} = 24.11$ Mg/ha). Although an opposite trend was found in high-severity sections of the burns (lower AGBD and canopy height changes in short-interval fire regions), insignificant differences ($p > 0.05$) were observed among samples with respect to fire frequency, suggesting dominant roles of high-severity fire on vegetation removal regardless of potential differences relative to fire-return intervals.

V. Discussion

In this research, multidate Lidar observations enabled a quantitative assessment of fire-induced forest structure and AGBD changes relative to independently generated burn severity levels. All the spectral indices (i.e., postfire NBR; dNBR; RdNBR) were found to correlate with relative canopy height and AGBD losses. Although the strength and significance of spectral-structural correlation varied among sites and wildfire events, dNBR

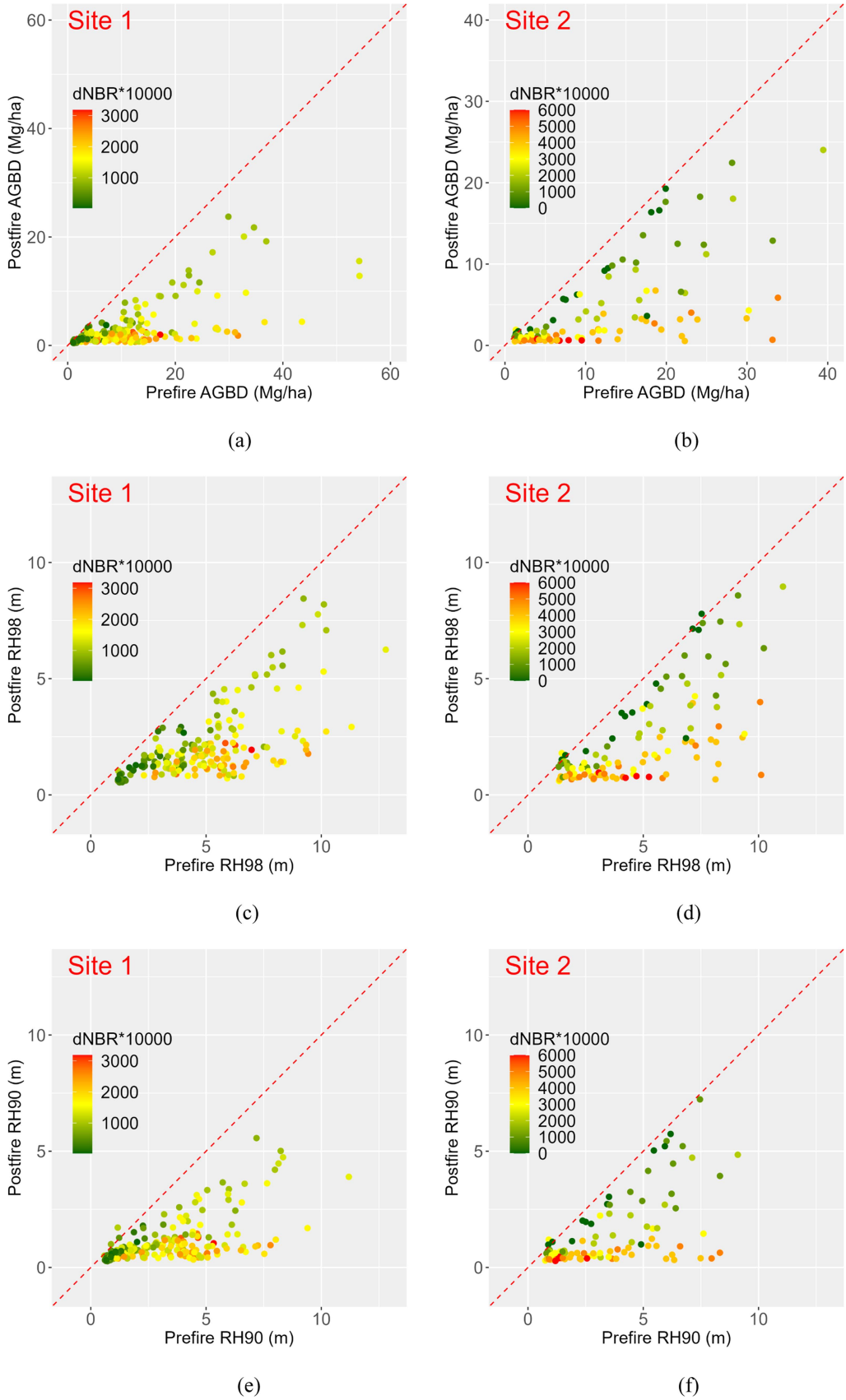

Fig. 5. Comparisons of AGBD (a; b) and multiple RH metrics (c; d; e; f; g; h; i; j; k; l; m; n) pre- and post-fire across a burn severity gradient.

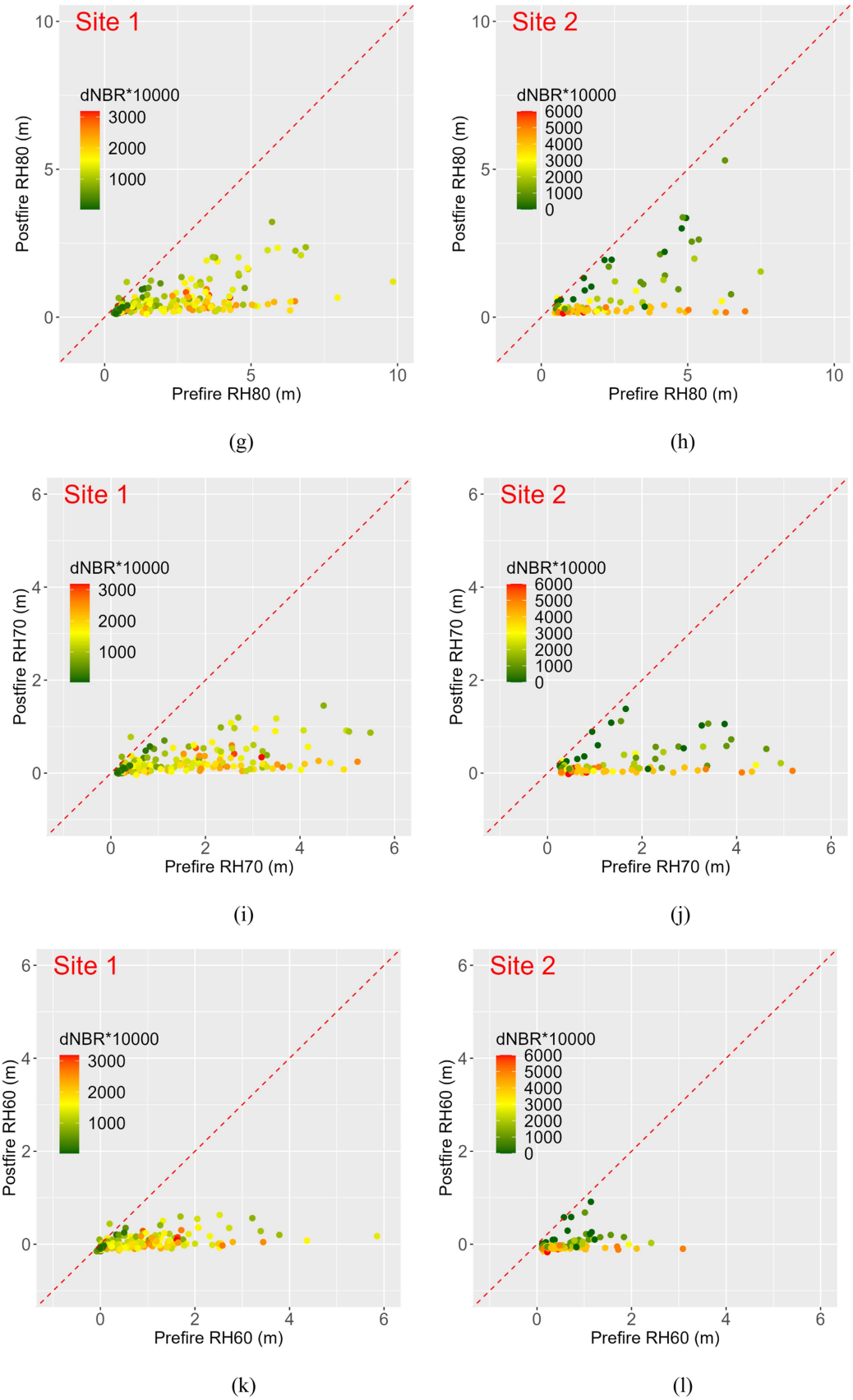

Fig. 5. *(Continued.)*

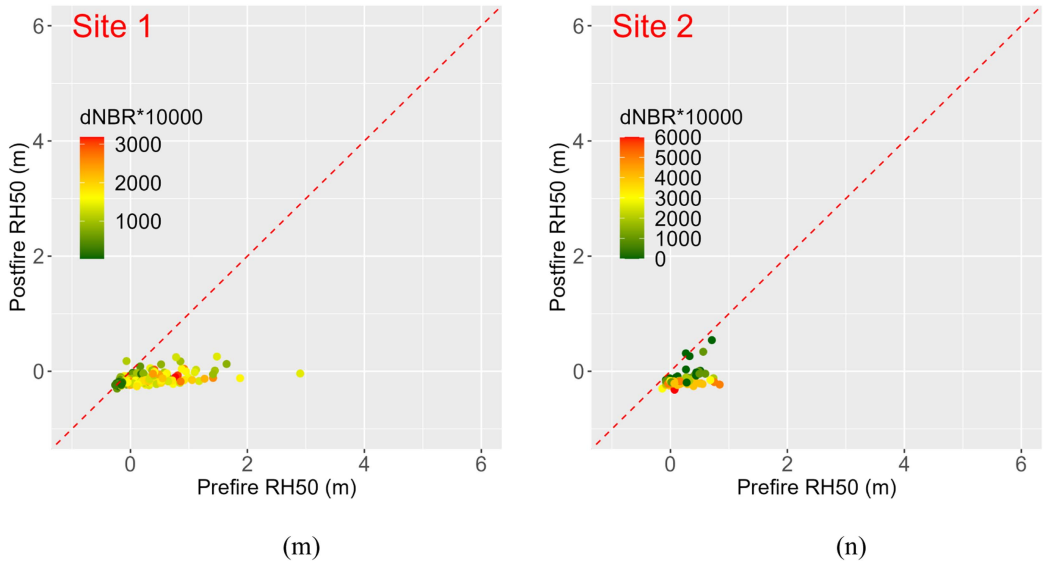

(m) (n)

Fig. 5. *(Continued.)*

TABLE IV
PIXEL-LEVEL COMPARISON OF PRE-, POST- AND ABSOLUTE CHANGE OF LIDAR METRICS WITHIN SITE 2 CHARACTERIZED BY LOW- AND HIGH-FIRE RETURN INTERVALS

Variable	Low fire-frequency region (Long fire-return intervals) Sample size = 1159			High Fire-frequency Region (Short fire-return intervals) Sample size = 2084			t-test		
	Prefire LiDAR	Postfire LiDAR	delta LiDAR metrics	Prefire LiDAR	Postfire LiDAR	delta LiDAR metrics	Prefire LiDAR (2010)	Postfire LiDAR	delta LiDAR metrics
AGBD (Mg/ha)	10.70	2.30	8.40	10.07	3.38	6.69	–1.64 (0.102)	**5.60 ($p < 0.001$)**	**–5.41 ($p < 0.001$)**
Canopy Height (m)	4.72	1.69	3.03	4.53	2.06	2.47	–1.78 (0.076)	**4.80 ($p < 0.001$)**	**–6.38 ($p < 0.001$)**
RH90 (m)	3.12	0.72	2.40	2.92	1.09	1.84	**–2.14 (0.032)**	**7.33 ($p < 0.001$)**	**–7.05 ($p < 0.001$)**
RH80 (m)	2.10	0.31	1.790	2.01	0.49	1.51	–1.26 (0.207)	**6.78 ($p < 0.001$)**	**–4.01 ($p < 0.001$)**
RH70 (m)	1.31	0.90	1.22	1.24	0.14	1.10	–1.29 (0.199)	**4.78 ($p < 0.001$)**	**–2.27 (0.024)**
RH60 (m)	0.59	-0.06	0.65	0.52	-0.05	0.57	**–2.64 (0.008)**	**3.47 ($p < 0.001$)**	**–3.27 (0.001)**
RH 50 (m)	0.17	-0.19	0.36	0.14	-0.19	0.33	**–2.88 (0.004)**	**2.30 (0.022)**	**–3.68 ($p < 0.001$)**

In bold: significant values with $p < 0.0001$ and $\alpha = 0.05$.

demonstrated a higher degree of correlations with fire-induced forest structural and AGBD change for both study sites. Over our two study sites in Canada, we observed that vegetation resistance to wildfire is highly strata- and burn severity-dependent. Within high-biomass stands with tall trees, the dominant trees occupying the upper canopy layer showed a lower degree of fire-induced loss (i.e., lower magnitude of change in AGBD and Lidar height metrics), while understory vegetation was more likely to experience full removal regardless of prefire condition and burn severity levels. We further assessed the impact of fire-return intervals on magnitudes of RH and AGBD changes, and found the postfire, absolute changes of all Lidar attributes were significantly different by site (fire frequency). The magnitudes of forest structure and aboveground biomass losses with respect to burn severity and fire-return intervals provide implications for forest recovery processes and carbon dynamics in boreal forests, a geographical domain with an accelerated prevalence of high-frequency wildfires projected [70], [71].

A. *Interpretation of Landsat-Derived Burn Severity Metrics*

Cautious interpretation of burn severity measurements from multispectral imagery has been recommended due to possible limitations as a scale-invariant proxy for specific burn severity biometrics [9], [42], [72]. The results found in our study supported this position, indicating the strength and significance of spectral indices for forest structure characterizations vary

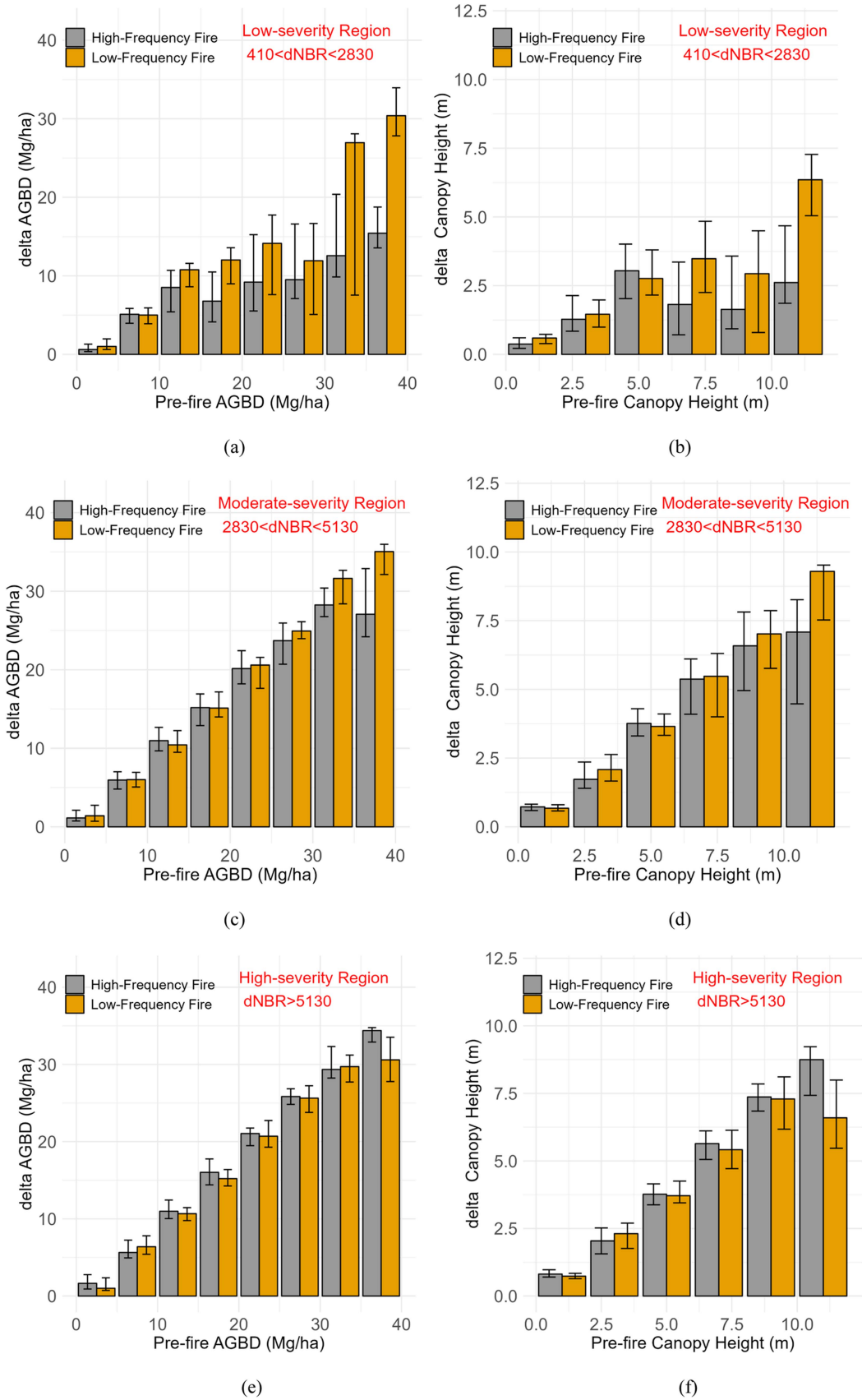

Fig. 6. Median, 25th and 75th percentile of delta AGBD (a); (c); (e) and canopy height (b); (d); (f) across pre-fire gradient within the perimeters of low- (a); (b), moderate- (c); (d) and high- (e); (f) severity fire.

between study sites. This could possibly be attributed to the substantial variability of species distribution [25], topography [73], and date of image selection [74], which are all considered to impact dNBR values. Coincident with results reported in [42], dNBR demonstrated stronger linkages with structural attributes in our study sites, especially those Lidar metrics representing the structural characteristics of upper canopy layers (i.e., RH98; RH90). RdNBR, the relative form of dNBR, showed a lower degree of agreement with Lidar attributes in both study sites. Through the analysis, we provided evidence that the Landsat-derived burn severity indices have the potential to characterize fire-induced forest structure change. The strong linkages between changes in spectral and structural signals in the wildfire examples theoretically support the extrapolation of forest structure and AGBD changes across space and time. We anticipated further efforts to integrate multispectral and Lidar observations for large-scale fire-induced forest structure change characterizations, which facilitates our direct assessments of long-term wildfire effects on forest losses and carbon cycle dynamics.

B. Multitemporal Lidar for Direct Assessment of Forest Structure Changes

The availability of multitemporal Lidar enables direct assessment of forest structure and AGBD changes through wildfire [41], [42]. One novelty in this work is an integration of multisensor Lidar for forest structure change observations pre- and postfire. Through a conversion from DRL to pseudo-LVIS waveform, we found a strong agreement for footprint-level terrain height pre- and postfire, as well as a sharp decrease of canopy height, which demonstrated the heterogeneous postfire effects on the forest canopy. The high coincidence of terrain elevation ($\text{RMSE}_{\text{site 1}} = 0.54$ m; $\text{bias}_{\text{site 1}} = 0.25$m; $\text{RMSE}_{\text{site 2}} = 0.28$; $\text{bias}_{\text{site 2}} = 0.13$ m) indicates the multitemporal Lidar data were properly collocated and the associated data could be used for change analysis. These results further support conclusions found in [57] and [62], highlighting the potential for combining multisourced and cross-platform Lidar for forest structure monitoring and change analysis. It should be noted that the primary methodological framework for the Lidar-based postfire effects assessment is by means of comparison between paired metrics pre- and postfire, thereby evaluating the wildfire effects on forest structure change. The rapid increase of Lidar availability acquired from air- and space-borne platforms provide further opportunities for a standardization of postfire effects assessment through the development of Lidar-based burn severity protocol. Compared to the assessment strategies adopted in the CBI protocol, utilisations of multitemporal Lidar can offer highly objective and detailed evaluations of wildfire effects on forest structure and AGBD dynamics on the aboveground portions. While some initial efforts have been made so far to incorporate multitemporal Lidar for fire damage assessments, the approaches adopted in previous studies either relied on correlations between CBI and Lidar attributes [75] or used single Lidar metrics to represent the burn severity level [76]. We recommended further efforts incorporating structural measurements across entire forest vertical profiles for a comprehensive illustration of wildfire effects on forest damages. As airborne Lidar becomes more readily available in boreal systems, e.g., through recent province-wide collections in Ontario, forthcoming province-wide collections in British Columbia, etc., there is an opportunity to assess change over wide areas, but only if multiple differing Lidar platforms can be directly compared. The approach presented in this article illustrates one methodological approach to fire damage assessment from disparate Lidar platforms that could be adopted for wider areas given future data availability.

C. Prefire Forest Structure and Burn Severity Levels

The prefire fuel structure and density were found to play a prominent role in fire behavior and subsequent postfire effects regulation [77]. This interrelation has been evaluated through prefire inventory and burn severity indices from multispectral imagery [9], [78], [79]. While associations were identified between prefire structural attributes (e.g., canopy height, stem density, AGBD, etc.) and spectral measurements (postfire NBR, dNBR, and RdNBR), correlations are found to be idiosyncratic to particular study sites and wildfire events. This can be attributed to 1) differences in species compositions and characteristics in terms of their fire tolerance levels, stand age, etcetera, and/or 2) limited usability of burn severity indices to characterize fire-induced forest structure and AGBD losses. In addition, the date of postfire Lidar survey can also impact the strength of this association. The temporal window between the date of wildfire (i.e., 2011 at the first site; 2013 at the second site) and postfire Lidar acquisition (2019) allows an extended assessment of wildfire effects, whereas the initial assessment through Lidar survey is prone to miss the standing dead residuals. Across both study sites, strong consistency was found in terms of the magnitude of forest structure and AGBD changes relative to burn severity and vertical distributions of vegetation at the prefire stage. Particularly, the strata-variant structural responses to wildfire provide additional insights for postfire effects assessment across entire forest vertical profiles. This finding also indicated the pressing need to integrate high-resolution forest vertical structure data as prefire inventory, in complement with optical-based measurements already existing [80], to better assist our remotely sensed wildfire effects evaluation and subsequent postfire recovery analysis.

D. Impacts of Fire-Return Interval on Forest Change

The postfire effects, as captured by changes in spectral indices and structural attributes, were identified to be significantly different across regions with short and long-interval fires. Comparatively, regions with previous burns demonstrated lower magnitudes of burn severity in subsequent wildfires, as depicted by the distributions of multispectral indices (i.e., postfire NBR, dNBR, and RdNBR). In parallel to the spectral analysis, we found the same conclusion from a structural perspective, indicating that areas with high-frequency wildfires were prone to experience lower degrees of damage, primarily in the low-severity section of the burns. This finding coincides with results found in previous studies [45], [81], which rely on multispectral burn severity measurements to evaluate the variabilities of postfire

effects relative to return-return intervals. Notably, our efforts of integrating multitemporal Lidar extend the scope of previous work and provide quantitative evidence of interactions among burn severity, fire-return intervals, and forest losses. We considered this variability of vegetation resistance to low-severity fire with respect to fire-return interval primarily attributed to the shift of conifer to deciduous-dominated successional trajectories as a result of multiple burns in the past few decades [14] while the fire-adapted black spruce that previously dominated this site experienced a density reduction and was replaced by trembling aspen given its rapid asexual regeneration strategies and competitive abilities at early successional stage [82]. The dominance of trembling aspen, along with its higher resistance to wildfire is considered a potential explanation that stands within short-interval fire perimeters displaying a lower canopy height loss rate and biomass combustion completeness under low-severity wildfire. Though this finding remains speculative due to the lack of field inventories pre- and postfire, we demonstrated the strong capacity of multitemporal Lidar to detect the variabilities of forest structure and AGBD losses relative to fire-return intervals and burn severity levels. We anticipate future work with the integration of repeated and species-specific stem measurements to further illuminate drivers of the interactions among fire-return intervals, and the magnitude of canopy height and AGBD changes.

VI. Conclusion

In this study, we examined the magnitudes of forest structure and AGBD changes through wildfires across two sites in the Canadian boreal forest. Burn severity indices from multitemporal Landsat demonstrated limited capacity to characterize forest structure change and the correlations between spectral indices and structural attributes were found to be idiosyncratic in terms of strength and significance. Magnitudes of forest structure and AGBD losses were highly dependent upon prefire conditions and burn severity. Specifically, tall trees in stands dominated by high AGBD showed higher resistance to low- and moderate-severity wildfires while understory vegetation occupying lower forest layers was less fire-tolerant and highly flammable, regardless of burn severity. We further explored the impact of fire-return intervals on the magnitude of forest structure and AGBD changes. Forests with the presence of previous burns were characterized by lower magnitudes of both absolute and relative changes in canopy height and AGBD), which were explained by impacts of previous burns. This work illuminates the interactions between fire-return intervals, burn severity, and heterogeneities of postfire effects on 3-D forest structure. Particularly, multitemporal Lidar facilitated quantitative assessments of structure change and carbon fluxes in a spatially explicit fashion. This study further strengthens our knowledge about wildfire impacts on forest structure dynamics and carbon feedback, which is of increasing importance given the increasing fire activities in boreal forests associated with climate change.

Acknowledgment

We express our gratitude for three anonymous reviewers who provide constructive comments to this manuscript. We thank the National Snow and Ice Data center and NASA ABoVE LVIS team for providing the LVIS datasets (https://nsidc.org/data/data-access-tool/LVISF2/versions/1; https://nsidc.org/data/data-access-tool/LVISF1B/versions/1). We also thank the USGS for providing Landsat data (https://glovis.usgs.gov/). We also express our appreciation for Natural Resources Canada for the National Burn Area Composite (https://cwfis.cfs.nrcan.gc.ca/datamart/download/nbac).

References

[1] E. S. Kasischke et al., "Alaska's changing fire regime — Implications for the vulnerability of its boreal forests. This article is one of a selection of papers from the dynamics of change in alaska's boreal forests: Resilience and vulnerability in response to climate warming," *Can. J. Forest Res.*, vol. 40, no. 7, pp. 1313–1324, Jul. 2010.

[2] C. Tymstra, B. J. Stocks, X. Cai, and M. D. Flannigan, "Wildfire management in Canada: Review, challenges and opportunities," *Prog. Disaster Sci.*, vol. 5, Jan. 2020, Art. no. 100045.

[3] B. J. Stocks et al., "Large forest fires in Canada, 1959–1997," *J. Geophysical Res.*, vol. 107, no. D1, pp. FFR 5–FFR 1–FFR 5–12, Jan. 2002, doi: 10.1029/2001jd000484.

[4] B. D. Amiro, B. J. Stocks, M. E. Alexander, M. D. Flannigan, and B. M. Wotton, "Fire, climate change, carbon and fuel management in the Canadian boreal forest," *Int. J. Wildland Fire*, vol. 10, no. 4, 2001, Art. no. 405.

[5] N. C. Coops, T. Hermosilla, M. A. Wulder, J. C. White, and D. K. Bolton, "A thirty year, fine-scale, characterization of area burned in Canadian forests shows evidence of regionally increasing trends in the last decade," *PLoS One*, vol. 13, no. 5, May 2018, Art. no. e0197218.

[6] M. S. Balshi et al., "The role of historical fire disturbance in the carbon dynamics of the pan-boreal region: A process-based analysis," *J. Geophysical Res.*, vol. 112, no. G2, Jun. 2007, doi: 10.1029/2006jg000380.

[7] E. S. Kasischke, N. L. Christensen Jr, and B. J. Stocks, "Fire, global warming, and the carbon balance of boreal forests," *Ecol. Appl.*, vol. 5, no. 2, pp. 437–451, May 1995.

[8] C. Tymstra, M. D. Flannigan, O. B. Armitage, and K. Logan, "Impact of climate change on area burned in Alberta's boreal forest," *Int. J. Wildland Fire*, vol. 16, no. 2, 2007, Art. no. 153.

[9] M. A. Wulder, J. C. White, F. Alvarez, T. Han, J. Rogan, and B. Hawkes, "Characterizing boreal forest wildfire with multi-temporal Landsat and LIDAR data," *Remote Sens. Environ.*, vol. 113, no. 7, pp. 1540–1555, Jul. 2009.

[10] C. H. Key and N. Benson, "Landscape assessment: Ground measure of severity, the composite burn index; and remote sensing of severity, the normalized burn ratio," in *FIREMON: Fire Effects Monitoring and Inventory System USDA Forest Service. (CD:LA1-LA51)*, D. C. Lutes, R. E. Keane, J. F. Caratti, C. H. Key, N. C. Benson, and L. J. Gangi, Eds. Ogden, UT, USA: United States Dept. Agric., 2005.

[11] M. G. Turner, W. L. Baker, C. J. Peterson, and R. K. Peet, "Factors influencing succession: Lessons from large, infrequent natural disturbances," *Ecosystems*, vol. 1, no. 6, pp. 511–523, Nov. 1998.

[12] J. K. Agee, *Fire Ecology of Pacific Northwest Forests*. WA, DC, USA: Island Press, 1995.

[13] E. Whitman, M.-A. Parisien, D. K. Thompson, R. J. Hall, R. S. Skakun, and M. D. Flannigan, "Variability and drivers of burn severity in the northwestern Canadian boreal forest," *Ecosphere*, vol. 9, no. 2, Feb. 2018, Art. no. e02128.

[14] J. F. Johnstone and F. S. Chapin III, "Fire interval effects on successional trajectory in boreal forests of northwest Canada," *Ecosystems*, vol. 9, no. 2, pp. 268–277, Mar. 2006.

[15] J. D. Coop et al., "Wildfire-driven forest conversion in western north American landscapes," *Bioscience*, vol. 70, no. 8, pp. 659–673, Aug. 2020.

[16] T. V. Loboda, N. H. F. French, C. Hight-Harf, L. Jenkins, and M. E. Miller, "Mapping fire extent and burn severity in Alaskan tussock tundra: An analysis of the spectral response of tundra vegetation to wildland fire," *Remote Sens. Environ.*, vol. 134, pp. 194–209, Jul. 2013.

[17] S. Veraverbeke, S. Lhermitte, W. W. Verstraeten, and R. Goossens, "The temporal dimension of differenced Normalized Burn Ratio (dNBR) fire/burn severity studies: The case of the large 2007 Peloponnese wildfires in Greece," *Remote Sens. Environ.*, vol. 114, no. 11, pp. 2548–2563, Nov. 2010.

[18] S. Escuin, R. Navarro, and P. Fernández, "Fire severity assessment by using NBR (Normalized Burn Ratio) and NDVI (Normalized Difference Vegetation Index) derived from LANDSAT TM/ETM images," *Int. J. Remote Sens.*, vol. 29, no. 4, pp. 1053–1073, Feb. 2008.

[19] J. C. White, M. A. Wulder, T. Hermosilla, N. C. Coops, and G. W. Hobart, "A nationwide annual characterization of 25 years of forest disturbance and recovery for Canada using Landsat time series," *Remote Sens. Environ.*, vol. 194, pp. 303–321, Jun. 2017.

[20] E. Alonso-González and V. Fernández-García, "MOSEV: A global burn severity database from MODIS (2000–2020)," *Earth Syst. Sci. Data*, vol. 13, no. 5, pp. 1925–1938, May 2021.

[21] D. P. Roy, Y. Jin, P. E. Lewis, and C. O. Justice, "Prototyping a global algorithm for systematic fire-affected area mapping using MODIS time series data," *Remote Sens. Environ.*, vol. 97, no. 2, pp. 137–162, Jul. 2005.

[22] J. D. Miller and A. E. Thode, "Quantifying burn severity in a heterogeneous landscape with a relative version of the delta Normalized Burn Ratio (dNBR)," *Remote Sens. Environ.*, vol. 109, no. 1, pp. 66–80, Jul. 2007.

[23] D. C. Lutes et al., "FIREMON: Fire effects monitoring and inventory system," U.S. Department of Agriculture, Forest Service, Rocky Mountain Research Station, Ft. Collins, CO, 2006, doi: 10.2737/rmrs-gtr-164.

[24] J. W. van Wagtendonk, K. A. van Wagtendonk, and A. E. Thode, "Factors associated with the severity of intersecting fires in Yosemite National Park, California, USA," *Fire Ecol.*, vol. 8, no. 1, pp. 11–31, Apr. 2012.

[25] J. L. Allen and B. Sorbel, "Assessing the differenced Normalized Burn Ratio's ability to map burn severity in the boreal forest and tundra ecosystems of Alaska's national parks," *Int. J. Wildland Fire*, vol. 17, no. 4, 2008, Art. no. 463.

[26] N. H. F. French et al., "Using Landsat data to assess fire and burn severity in the North American boreal forest region: An overview and summary of results," *Int. J. Wildland Fire*, vol. 17, no. 4, 2008, Art. no. 443.

[27] R. J. Hall, J. T. Freeburn, W. J. de Groot, J. M. Pritchard, T. J. Lynham, and R. Landry, "Remote sensing of burn severity: Experience from western Canada boreal fires," *Int. J. Wildland Fire*, vol. 17, no. 4, 2008, Art. no. 476.

[28] E. E. Hoy, N. H. F. French, M. R. Turetsky, S. N. Trigg, and E. S. Kasischke, "Evaluating the potential of Landsat TM/ETM+ imagery for assessing fire severity in Alaskan black spruce forests," *Int. J. Wildland Fire*, vol. 17, no. 4, 2008, Art. no. 500.

[29] N. O. Soverel, D. D. B. Perrakis, and N. C. Coops, "Estimating burn severity from Landsat dNBR and RdNBR indices across western Canada," *Remote Sens. Environ.*, vol. 114, no. 9, pp. 1896–1909, Sep. 2010.

[30] J. W. van Wagtendonk, R. R. Root, and C. H. Key, "Comparison of AVIRIS and Landsat ETM+ detection capabilities for burn severity," *Remote Sens. Environ.*, vol. 92, no. 3, pp. 397–408, Aug. 2004.

[31] J. E. Keeley, "Fire intensity, fire severity and burn severity: A brief review and suggested usage," *Int. J. Wildland Fire*, vol. 18, no. 1, 2009, Art. no. 116.

[32] A. Lü, H. Tian, M. Liu, J. Liu, and J. M. Melillo, "Spatial and temporal patterns of carbon emissions from forest fires in China from 1950 to 2000," *J. Geophysical Res.*, vol. 111, no. D5, 2006, doi: 10.1029/2005jd006198.

[33] J. B. Drake, R. O. Dubayah, R. G. Knox, D. B. Clark, and J. B. Blair, "Sensitivity of large-footprint Lidar to canopy structure and biomass in a neotropical rainforest," *Remote Sens. Environ.*, vol. 81, no. 2–3, pp. 378–392, Aug. 2002.

[34] M. A. Lefsky, W. B. Cohen, D. J. Harding, G. G. Parker, S. A. Acker, and S. T. Gower, "Lidar remote sensing of above-ground biomass in three biomes," *Glob. Ecol. Biogeogr.*, vol. 11, no. 5, pp. 393–399, Sep. 2002.

[35] R. Dubayah et al., "The global ecosystem dynamics investigation: High-resolution laser ranging of the Earth's forests and topography," *Sci. Remote Sens.*, vol. 1, Jun. 2020, Art. no. 100002.

[36] L. Duncanson et al., "Aboveground biomass density models for NASA's Global Ecosystem Dynamics Investigation (GEDI) Lidar mission," *Remote Sens. Environ.*, vol. 270, Mar. 2022, Art. no. 112845.

[37] M. A. Wulder, T. Han, J. C. White, T. Sweda, and H. Tsuzuki, "Integrating profiling Lidar with Landsat data for regional boreal forest canopy attribute estimation and change characterization," *Remote Sens. Environ.*, vol. 110, no. 1, pp. 123–137, Sep. 2007.

[38] K. Zhao, J. C. Suarez, M. Garcia, T. Hu, C. Wang, and A. Londo, "Utility of multitemporal Lidar for forest and carbon monitoring: Tree growth, biomass dynamics, and carbon flux," *Remote Sens. Environ.*, vol. 204, pp. 883–897, Jan. 2018.

[39] Y. K. Karna, T. D. Penman, C. Aponte, N. Hinko-Najera, and L. T. Bennett, "Persistent changes in the horizontal and vertical canopy structure of fire-tolerant forests after severe fire as quantified using multi-temporal airborne Lidar data," *Forest Ecol. Manage.*, vol. 472, Sep. 2020, Art. no. 118255.

[40] M. Alonzo, D. C. Morton, B. D. Cook, H.-E. Andersen, C. Babcock, and R. Pattison, "Patterns of canopy and surface layer consumption in a boreal forest fire from repeat airborne Lidar," *Environ. Res. Lett.*, vol. 12, no. 6, May 2017, Art. no. 065004.

[41] T. Hu et al., "A simple and integrated approach for fire severity assessment using bi-temporal airborne Lidar data," *Int. J. Appl. Earth Observ. Geoinf.*, vol. 78, pp. 25–38, Jun. 2019.

[42] T. R. McCarley et al., "Multi-temporal Lidar and Landsat quantification of fire-induced changes to forest structure," *Remote Sens. Environ.*, vol. 191, pp. 419–432, Mar. 2017.

[43] D. K. Bolton, N. C. Coops, and M. A. Wulder, "Characterizing residual structure and forest recovery following high-severity fire in the western boreal of Canada using Landsat time-series and airborne Lidar data," *Remote Sens. Environ.*, vol. 163, pp. 48–60, Jun. 2015.

[44] B. J. Harvey, D. C. Donato, and M. G. Turner, "Burn me twice, shame on who? Interactions between successive forest fires across a temperate mountain region," *Ecology*, vol. 97, no. 9, pp. 2272–2282, Sep. 2016.

[45] S. A. Parks, C. Miller, C. R. Nelson, and Z. A. Holden, "Previous fires moderate burn severity of subsequent wildland fires in two large western US wilderness areas," *Ecosystems*, vol. 17, no. 1, pp. 29–42, Jan. 2014.

[46] G. Matasci et al., "Large-area mapping of Canadian boreal forest cover, height, biomass and other structural attributes using Landsat composites and Lidar plots," *Remote Sens. Environ.*, vol. 209, pp. 90–106, May 2018.

[47] T. Hermosilla, M. A. Wulder, J. C. White, and N. C. Coops, "Prevalence of multiple forest disturbances and impact on vegetation regrowth from interannual Landsat time series (1985–2015)," *Remote Sens. Environ.*, vol. 233, Nov. 2019, Art. no. 111403.

[48] L. A. Venier et al., "Effects of natural resource development on the terrestrial biodiversity of Canadian boreal forests," *Environ. Rev.*, vol. 22, no. 4, pp. 457–490, Dec. 2014.

[49] I. B. Marshall, C. A. Scott Smith, and C. J. Selby, "A national framework for monitoring and reporting on environmental sustainability in Canada," *Environ. Monit. Assessment*, vol. 39, no. 1–3, pp. 25–38, Jan. 1996.

[50] H. E. Beck, N. E. Zimmermann, T. R. McVicar, N. Vergopolan, A. Berg, and E. F. Wood, "Present and future Köppen-Geiger climate classification maps at 1-km resolution," *Sci. Data*, vol. 5, no. 1, Oct. 2018, Art. no. 180214.

[51] E. Canada, Canadian Climate Normals 1981-2010 Station Data. Accessed: Mar. 4, 2026. [Online]. Available: https://climate.weather.gc.ca/climate_normals/results_1981_2010_e.html?searchType=stnProv&lstProvince=SK&txtCentralLatMin=0&txtCentralLatSec=0&txtCentralLongMin=0&txtCentralLongSec=0&stnID=3360&dispBack=0

[52] T. Hermosilla, A. Bastyr, N. C. Coops, J. C. White, and M. A. Wulder, "Mapping the presence and distribution of tree species in Canada's forested ecosystems," *Remote Sens. Environ.*, vol. 282, Dec. 2022, Art. no. 113276.

[53] R. Skakun et al., "Extending the national burned area composite time series of wildfires in Canada," *Remote Sens. (Basel)*, vol. 14, no. 13, Jun. 2022, Art. no. 3050.

[54] M. A. Wulder, J. C. White, C. W. Bater, N. C. Coops, C. Hopkinson, and G. Chen, "Lidar plots — A new large-area data collection option: Context, concepts, and case study," *Can. J. Remote Sens./J. Canadien Télédétection*, vol. 38, no. 5, pp. 600–618, Nov. 2012.

[55] C. Hopkinson, M. A. Wulder, N. C. Coops, T. Milne, A. Fox, and C. B. Bater, "Airborne Lidar sampling of the Canadian boreal forest: Planning, execution & initial processing," in *Proc. SilviLaser*, 2011.

[56] C. E. Miller et al., "An overview of ABoVE airborne campaign data acquisitions and science opportunities," *Environ. Res. Lett.*, vol. 14, no. 8, Aug. 2019, Art. no. 080201.

[57] S. Hancock et al., "The GEDI simulator: A large-footprint waveform Lidar simulator for calibration and validation of spaceborne missions," *Earth Space Sci.*, vol. 6, no. 2, pp. 294–310, Feb. 2019.

[58] J. B. Blair and M. Hofton, "LVIS facility L1B geolocated return energy waveforms, version 1," NASA National Snow and Ice Data Center DAAC, 2020, doi: 10.5067/XQJ8PN8FTIDG.

[59] J. B. Blair and M. Hofton, "LVIS facility L2 geolocated surface elevation product, version 1," NASA National Snow and Ice Data Center DAAC, 2020, doi: 10.5067/VP7J20HJQISD.

[60] T. V. Loboda, D. Chen, J. V. Hall, and J. He, "ABoVE: Landsat-derived burn scar dNBR across Alaska and Canada, 1985-2015," ORNL Distributed Active Archive Center, 2018, doi: 10.3334/ORNLDAAC/1564.

[61] J. B. Blair and M. A. Hofton, "Modeling laser altimeter return waveforms over complex vegetation using high-resolution elevation data," *Geophys. Res. Lett.*, vol. 26, no. 16, pp. 2509–2512, Aug. 1999.

[62] C. A. Silva et al., "Comparison of small- and large-footprint Lidar characterization of tropical forest aboveground structure and biomass: A case study from central Gabon," *IEEE J. Sel. Topics Appl. Earth Observ. Remote Sens.*, vol. 11, no. 10, pp. 3512–3526, Oct. 2018.
[63] P. M. Montesano, M. J. Macander, and E. E. Hoy, "ABoVE: LVIS L3 gridded vegetation structure across Alaska and Canada, 2017 and 2019," ORNL Distributed Active Archive Center, May 2022, doi: 10.3334/ORNLDAAC/1923.
[64] C. J. Tucker, "Red and photographic infrared linear combinations for monitoring vegetation," *Remote Sens. Environ.*, vol. 8, no. 2, pp. 127–150, May 1979.
[65] Y. Cheng, "Mean shift, mode seeking, and clustering," *IEEE Trans. Pattern Anal. Mach. Intell.*, vol. 17, no. 8, pp. 790–799, Aug. 1995.
[66] D. Comaniciu and P. Meer, "Mean shift: A robust approach toward feature space analysis," *IEEE Trans. Pattern Anal. Mach. Intell.*, vol. 24, no. 5, pp. 603–619, May 2002.
[67] A. A. López-Caloca, "Data fusion approach for employing multiple classifiers to improve lake shoreline analysis," in *Advanced Information Systems Engineering*, in Lecture notes in computer science. Berlin, Germany: Springer, 2014, pp. 1022–1029.
[68] S. Bo, L. Ding, H. Li, F. Di, and C. Zhu, "Mean shift-based clustering analysis of multispectral remote sensing imagery," *Int. J. Remote Sens.*, vol. 30, no. 4, pp. 817–827, Feb. 2009.
[69] P. M. Montesano et al., "Patterns of regional site index across a North American boreal forest gradient," *Environ. Res. Lett.*, vol. 18, no. 7, Jul. 2023, Art. no. 075006.
[70] N. P. Gillett, "Detecting the effect of climate change on Canadian forest fires," *Geophys. Res. Lett.*, vol. 31, no. 18, 2004, doi: 10.1029/2004gl020876.
[71] S. Veraverbeke et al., "Lightning as a major driver of recent large fire years in North American boreal forests," *Nature Climate Change*, vol. 7, no. 7, pp. 529–534, Jul. 2017.
[72] C. A. Kolden, A. M. S. Smith, and J. T. Abatzoglou, "Limitations and utilisation of monitoring trends in burn severity products for assessing wildfire severity in the USA," *Int. J. Wildland Fire*, vol. 24, no. 7, 2015, Art. no. 1023.
[73] D. L. Verbyla, E. S. Kasischke, and E. E. Hoy, "Seasonal and topographic effects on estimating fire severity from Landsat TM/ETM+ data," *Int. J. Wildland Fire*, vol. 17, no. 4, 2008, Art. no. 527.
[74] D. Chen, T. V. Loboda, and J. V. Hall, "A systematic evaluation of influence of image selection process on remote sensing-based burn severity indices in North American boreal forest and tundra ecosystems," *ISPRS J. Photogrammetry Remote Sens.*, vol. 159, pp. 63–77, Jan. 2020.
[75] M. García et al., "Evaluating the potential of Lidar data for fire damage assessment: A radiative transfer model approach," *Remote Sens. Environ.*, vol. 247, Sep. 2020, Art. no. 111893.
[76] C. Wang and N. F. Glenn, "Estimation of fire severity using pre- and post-fire Lidar data in sagebrush steppe rangelands," *Int. J. Wildland Fire*, vol. 18, no. 7, 2009, Art. no. 848.
[77] S. F. Arno, "Fire ecology of pacific northwest forests, by J.K. Agee," *Int. J. Wildland Fire*, vol. 4, no. 3, 1994, Art. no. 195.
[78] A. M. Kuenzi, P. Z. Fulé, and C. H. Sieg, "Effects of fire severity and pre-fire stand treatment on plant community recovery after a large wildfire," *Forest Ecol. Manage.*, vol. 255, no. 3–4, pp. 855–865, Mar. 2008.
[79] O. Viedma, F. Chico, J. J. Fernández, C. Madrigal, H. D. Safford, and J. M. Moreno, "Disentangling the role of prefire vegetation vs. burning conditions on fire severity in a large forest fire in SE Spain," *Remote Sens. Environ.*, vol. 247, Sep. 2020, Art. no. 111891.
[80] M. A. Crowley et al., "Towards a whole-system framework for wildfire monitoring using Earth observations," *Glob. Change Biol.*, vol. 29, no. 6, pp. 1423–1436, Mar. 2023.
[81] R. S. Arkle, D. S. Pilliod, and J. L. Welty, "Pattern and process of prescribed fires influence effectiveness at reducing wildfire severity in dry coniferous forests," *Forest Ecol. Manage.*, vol. 276, pp. 174–184, Jul. 2012.
[82] J. L. Baltzer et al., "Increasing fire and the decline of fire adapted black spruce in the boreal forest," *Proc. Nat. Acad. Sci. USA*, vol. 118, no. 45, Nov. 2021, Art. no. e2024872118.

Tuo Feng is currently working toward the Ph.D. degree in geographical sciences from University of Maryland, College Park MD, USA.

His research interests include integration of air-, space-borne Lidar, and multispectral remote sensing for spatial-temporal assessment of forest carbon fluxes, and their relevance to climate change and wildfire disturbance regimes over boreal ecosystems.

Laura Duncanson received the Ph.D. degree in geographical sciences from University of Maryland, College Park.

She is an Assistant Professor with the University of Maryland, College Park, MD, USA. She uses Lidar data to understand and monitor forest carbon dynamics at local to global scales. She coleads the development of empirical biomass models for NASA missions (GEDI and ICESat 2) and is involved in several international efforts aimed at bringing consistency and transparency to the field of remote sensing of forest biomass.

Steven Hancock received the M.Sci. degree in physics from the University of Durham, Durham, U.K., in 2005, and the Ph.D. degree in space and climate physics from University College, London, U.K., in 2010.

He is currently an Associate Professor with the School of Geosciences, University of Edinburgh, the Director of the NERC Field Spectroscopy Facility, and member of the National Centre for Earth Observation. He mainly works on Lidar remote sensing. This has included being a member of the GEDI science team, collaborating on a number of GEDI and ICESat-2 projects, and leading the UKSA GLAMIS project.

Paul Montesano received the Ph.D. degree in geographical sciences from University of Maryland, College Park.

He is a Research Scientist focusing on the use of remote sensing and geospatial data integration to examine earth system processes. He collaborates with interdisciplinary research teams on projects that use NASA and commercial spaceborne and airborne remote sensing data along with physical models and field observations to understand ecosystem processes.

Sergii Skakun received the M.S. degree (Hons.) in applied mathematics from the Physics and Technology Institute, NTUU "Kyiv Polytechnic Institute," Kyiv, Ukraine, in 2004, and the Ph.D. degree in computer science from the National Academy of Sciences of Ukraine, Kyiv, Ukraine, in 2005.

He is an Associate Professor with the Department of Geographical Sciences and College of Information Studies (iSchool), University of Maryland, College Park, MD, USA, and a Research Scientist with Terrestrial Information Systems Laboratory, NASA Goddard Space Flight Center (GSFC), Greenbelt, MD, USA. His research interests include advancing methods, models, and emerging technologies in the area of data science for heterogeneous remote sensing data fusion, processing, and analysis, and their applications to the areas of societal benefit.

Dr. Skakun is an Associate Editor of the journal *Remote Sensing of Environment*.

Michael A. Wulder received the Ph.D. degree in geography from the University of Waterloo, Waterloo, ON, Canada, in 1998.

He is a Senior Research Scientist with the Canadian Forest Service of Natural Resources Canada. He uses remotely sensed and spatial data to study and monitor forests across Canada, over a range of scales, contributing to national and international programs. He has worked with the Canadian Forest Service, Pacific Forestry Centre, in Victoria, British Columbia. His research efforts cover a range of scales from the plot- to the national scale, with data sources including Lidar to a range of optical satellites, leading to novel and open access map products of Canada's forest land cover, change, and structure. His major research publications include the book Remote Sensing of Forest Environments: Concepts and Case Studies (2003) and Forest Disturbance and Spatial Pattern: Remote Sensing and GIS Approaches (2006); with publication of more than 400 articles in peer-reviewed journals that have been cited $>$49 000 times with an h-index of $>$105 (Scholar Google). He is an adjunct Professor with the Department of Forest Resources Management of the University of British Columbia. He is a member of the USGS/NASA Landsat Science Team (since 2006) and played a lead role in initiating the SilviLaser series of international conferences focused on laser remote sensing of forest environments, and co-chaired the 2002 and 2012 editions.

Dr. Wulder was the recipient of the Gold Medal from the Canadian Remote Sensing Society for career excellence in remote sensing, in 2021. He was a Member of the Order of Canada for scientific achievements of national importance, in 2023.

Joanne C. White received the Doctor of Science degree in forest ecology and management from the Department of Forest Sciences, Faculty of Agriculture and Forestry, University of Helsinki, Helsinki, Finland, in 2019.

She is currently a Research Scientist with the Canadian Forest Service, Pacific Forestry Centre, Victoria, BC, Canada, and is also an Adjunct Professor with the Faculty of Forestry, University of British Columbia, BC, Canada. She has authored or coauthored more than 225 peer-reviewed publications (h-index 60). Her research interests include remote sensing applications for forest inventory and forest monitoring, primarily using airborne laser scanning and earth observation time series data.

Dr. White is the recipient of the Silver Medal by the Canadian Remote Sensing Society for her significant mid-career achievements in the field of remote sensing in Canada, in 2022. Since 2019, she has been named on the annual Web of Science global list of Highly Cited Researchers in both the cross-field and geosciences categories.

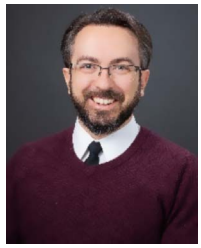

David Minor is a Research Scientist with the University of Maryland, College Park, MD, USA, involved in mapping forest structure from spaceborne Lidar. His research interests focuses on the calibration and validation of global biomass maps using data forest measurement plots and airborne Lidar.

Tatiana Loboda received the B.A. degree in geography and english from the Moscow State Pedagogical State University, Moscow, Russia, in 1995 and M.S. and Ph.D. degrees in geographical sciences from the University of Maryland, College Park, MD, USA, in 2004 and 2008, respectively.

She is an expert in Geospatial Data Science and works extensively with satellite observations, space-time modeling, climate change science, wildfire mapping and monitoring, and health applications. Her work on wildfires includes mapping fire extent, assessing fire progression, forecasting fire occurrence in the high northern latitudes, and assessing the impact of fire-driven air pollution on human health. She is engaged with diverse interdisciplinary teams of scientists, fire and resource management experts, and public health specialists in developing approaches to bringing Earth observations into the mainstream of land management and the broader context of public health and well-being. Her research interests include split between developing methods for wildfire risk and impact assessment and modeling and forecasting outbreaks of climate-sensitive infectious diseases.